



Impact of emission reduction on aerosol-radiation interaction during heavy pollution periods over Beijing-Tianjin-Hebei region in China

Wei Wen^{a,b}, Chunwei Guo^{a,*}, Xin Ma^c, Xiujuan Zhao^{a,*}, Lei Liu^d, Dan Chen^a, Jing Xu^a

^a Institute of Urban Meteorology, China Meteorological Administration, Beijing 100089, China

^b School of Energy and Environmental Engineering, University of Science and Technology Beijing, Beijing 100083, China

^c National Meteorological Center, Beijing 100081, China

^d Key Laboratory of Atmospheric Chemistry, China Meteorological Administration, Beijing 100081, China

ARTICLE INFO

Article history:

Received 28 September 2019

Revised 7 February 2020

Accepted 17 March 2020

Available online 4 May 2020

Keywords:

Aerosol-radiation interaction

Emission reduction

Meteorological factors

Pollutant concentration

ABSTRACT

In December 2015, the Beijing-Tianjin-Hebei (BTH) region experienced several episodes of heavy air pollution. The government immediately issued emergency control measures to reduce the pollution, which provided a good opportunity to explore the impact of emission reduction on aerosol-radiation interaction. In this study, four tests were conducted, including the base1 simulation with emission reduction and aerosol-radiation interaction on, the base2 simulation with emission reduction and aerosol-radiation interaction off, the scenario1 simulation without emission reduction and aerosol-radiation interaction on and the scenario2 simulation without emission reduction and aerosol-radiation interaction off. We find that the aerosol-radiation interaction decreased the downward shortwave radiation and the temperature at 2 m, reduced the planetary boundary layer height (PBLH) in the region, and increased the relative humidity at 2 m, which is favorable for pollution accumulation. Our results revealed that the interaction effect due to emission reductions increased downward shortwave radiation by an average of 0–5 W/m², leading to increase in surface temperature of 0–0.05°C, increase in the daytime mean PBL high of 0–8 m, and decrease in daytime mean relative humidity at 2 m of 0.5%. We found that if there were aerosol-radiation interaction, it would enhance the effectiveness of emission control measures on air pollution control. The enhancement of PM_{2.5} (particulate matter less than 2.5 μm), PM₁₀ (particulate matter less than 10 μm), and NO₂ (nitrogen dioxide) emission reduction effects reached 7.62%, 6.90%, 11.62%, respectively, over this region.

© 2020 Published by Elsevier B.V. on behalf of The Research Centre for Eco-Environmental Sciences, Chinese Academy of Sciences.

Introduction

Air pollution is a severe environmental problem in China (Kang et al., 2016; Li and Han, 2016; Kanaya et al., 2017). It poses a considerable threat to human health and affects climate change (Cao et al., 2012; Lang et al., 2017; Sharma and Balasubramanian, 2018; Ma et al., 2019). Aerosols can scatter (i.e., sulfate) and absorb (i.e., black carbon (BC)) solar radiation, which will affect the solar radiation in the atmosphere and the temperature at the surface (Santos et al., 2008; Dhar et al., 2017; Obregón et al., 2018). This effect is called the aerosol-radiation interaction. The aerosol-radiation interaction can cause changes in photolysis rates of photochemistry and regional meteorological factors, which affect air pollutants dispersion (Charlson et al., 1992; Pere et al., 2011; Boucher et al., 2013; Xing et al., 2015; Guo et al., 2016; Dong et al., 2018).

The Chinese government has made great efforts to reduce air pollution. A series of air pollution control plans have been issued by both central and local Chinese governments to effectively control regional PM_{2.5} (particulate matter less than 2.5 μm) pollution and improve air quality. The emission controls include the normal regulation of emission reduction and the emergency emission reduction. For example, in 2014 and 2015, the government ensured that the Asia-Pacific Economic Cooperation (APEC) meeting and the 70th anniversary of the Anti-Japanese War victory were successfully held when pollution levels were low. Emission controls have been correspondingly implemented in Beijing and the surrounding provinces (Hebei, Shaanxi, Inner Mongolia, Shandong, and Henan Provinces) (Wen et al., 2016; Wang et al., 2017). These emission controls provided experimental opportunities to explore the impact of emission controls on air pollution. For example, during the 2008 Olympic Games, the primary pollutants were significantly reduced, while the secondary pollutants increased after the full emission controls (Zhang et al., 2009; Wang et al., 2010).

* Corresponding authors.

E-mail addresses: cwguo@ium.cn (C. Guo), xjzhao@ium.cn (X. Zhao).

During the APEC period, the secondary aerosols had the greatest reductions, while the primary aerosols experienced a smaller change (Xu et al., 2015; Sun et al., 2016). These results highlighted the different responses of aerosol chemistry to emission controls.

In recent years, more attention has been paid to the potential feedback of aerosols to meteorological factors. There are increasing applications of online coupled models (i.e. WRF-Chem (weather research and forecasting model with chemistry)) on the study of aerosol feedbacks (Gao et al., 2014, 2016; Toll and Männik, 2015; Kalenderski and Stenchikov, 2016; Wang et al., 2018; Rizza et al., 2018; Goto et al., 2019; Hirti et al., 2019). Makar et al. (2015) found that temporal and spatial changes in the forecasted predictions of meteorological variables were due to direct and indirect aerosol feedbacks, with the largest impacts occurring in the summer and near large sources of pollution. The impacts of the changes in temperature, boundary layer height, and clouds that were triggered by the direct effect of aerosols on radiation were found to dominate the direct effect of aerosol particles on solar radiation (Forkel et al., 2012). Zhang et al. (2010) applied WRF-Chem and found that aerosols could reduce incoming solar radiation by up to 9% in January and 16% in July over most of the continental USA. At the same time, 2-m temperatures can be reduced by up to 0.16°C in January and 0.37°C in July. Although a few studies have investigated the influence of aerosol-radiation interactions on regional climate change in China (e.g., He et al., 2015; Leng et al., 2016; Zhang et al., 2016; Zhong et al., 2018), our knowledge of the impact of emission reduction on aerosol-radiation interactions in the Beijing-Tianjin-Hebei (BTH) region are far from complete. Knowing how these interactions may impact the response of air pollution to emission reductions and thus the effectiveness of emission control measures is necessary. The feedbacks induced by emission controls must be considered to understand the complex relationship between air quality and climate.

In December 2015, the Beijing-Tianjin-Hebei (BTH) region experienced several episodes of heavy air pollution. As an emergency response to pollution situations, the government immediately issued emergency control measures to reduce the pollution. This scenario provided experimental opportunities to explore how aerosol-radiation interactions respond to temporary emission control measures. In this work, the fully coupled online model WRF-Chem was applied to investigate this issue with a focus on aerosol-radiation interactions in the BTH region during the week of pollution. This work presents a regional-scale sensitivity study performed with WRF-Chem, with the purpose to emphasizing the need to account for aerosol-meteorology interactions when designing emission control measures and assessing their effectiveness.

1. Materials and methods

1.1. Model description

The fully coupled chemical transport on-line model (WRF-Chem, version 3.4.1) was used in this study. The physics options include the New Thompson microphysics scheme (Thompson et al., 2008), the Goddard shortwave scheme (Chou and Surare, 1994), the rapid radiative transfer model (RRTM) longwave radiation scheme (Mlawer et al., 1997), and the Yonsei University (YSU) planetary boundary layer (PBL) scheme (Hong et al., 2006). Carbon Bond mechanism version Z (CBM-Z, Zaveri and Peters, 1999) was used to calculate the gas phase chemistry, which consists of 67 prognostic species and 164 reactions. The aerosol module used was the model for simulating aerosol interactions and chemistry (MO-SAIC) (Zaveri et al., 2008). MOSAIC includes sulfate, methane, sulfonate, nitrate, chloride, carbonate, ammonium, sodium, calcium, black carbon (BC), primary organic mass (OC), liquid water, and

other inorganic mass (OIN) (e.g., trace metals, silica and other inert minerals). The module can simulate major aerosol processes (e.g., inorganic aerosol thermodynamic equilibrium, binary nucleation, coagulation, condensation, the particulate matter formation due to aqueous-phase chemistry, aerosol scavenged by cloud droplets, and dry and wet deposition) other than for secondary organic aerosol formation. In MOSAIC, the particle size distribution is simulated for four size bins (0.039–0.1, 0.1–1.0, 1.0–2.5, and 2.5–10 μm). The model calculated biogenic emission online using Gunther scheme. The direct effect of aerosols on shortwave radiation is simulated based on Mie theory following the approach of Fast et al. (2006).

1.2. Simulation configurations and design

The modeling domain covers a portion of northern China with 223 × 202 horizontal grid cells (as shown in Fig. 1). The horizontal resolution is 9 km. Thirty logarithmic structure layers divide the modeling vertical resolution, which ranges from the surface to a fixed pressure of 100 mb. The National Centers for Environmental Prediction (NCEP) Final Analysis Reanalysis data are used to generate the meteorology initial and boundary conditions. The 0.25° MEIC (the multi-resolution emission inventory for China) emission inventory of the year 2014 was used as the anthropogenic emission input (<http://meicmodel.org>). The model was applied for a 35-day period in Beijing, starting on November 25 and ending on December 31, 2015. The first 5 days were considered as the spin-up time and were excluded from the analysis.

The red alert represents the highest level of alert in response to heavy pollution, when mean hourly PM_{2.5} concentration over 150 μg/m³ lasts for over three days. During the red alert period, corresponding air pollution control measures are required. The control measures include public health protection measures, recommended control measures, and compulsory control measures. Public health protection measures include avoiding outdoor activities, expert interpretation and information publicity, and wearing masks. Recommended measures include canceling all large outdoor activities and closing all schools. Compulsory measures include suspending all construction projects, implementing even and odd-numbered license plates policy, and suspending the operation of more industrial plants. The first red alert was issued by Beijing municipal government on December 8 and was canceled on December 10. The second red alert was issued on December 19 and canceled on December 22, when the air quality was considerably improved in the region. The emergency control measures were implemented immediately in Beijing and the surrounding provinces. The emission reduction inventory was mainly updated based on municipal environmental protection bureaus and the implementation of emergency control measures during the 2 red alert periods (Jia et al., 2017). Three emission categories were updated, including industrial (industry sources), traffic (transportation sources), others (others, including coal-burning, power, etc.). Details of the reduction emission inventory can be found in Table 1.

In this research, several sensitivity simulations were conducted by turning on/off aerosol-radiation interaction and with/without emission reduction to investigate the impact of emission reduction on aerosol-radiation interaction. Scenario base1 was designed to represent the actual pollution process in Beijing during December 2015. Various emergency control measures were implemented and the direct aerosol feedback was activated. The simulation results from Scenario base1 were used for model verification. The base1 simulation was with emission reduction and the aerosol-radiation interaction turn on. The base2 simulation was with emission reduction and the aerosol-radiation interaction was turned off. The scenario1 simulation was without emission reduction and the aerosol-radiation interaction was turned on. The scenario2 simulation was without emission reduction and the

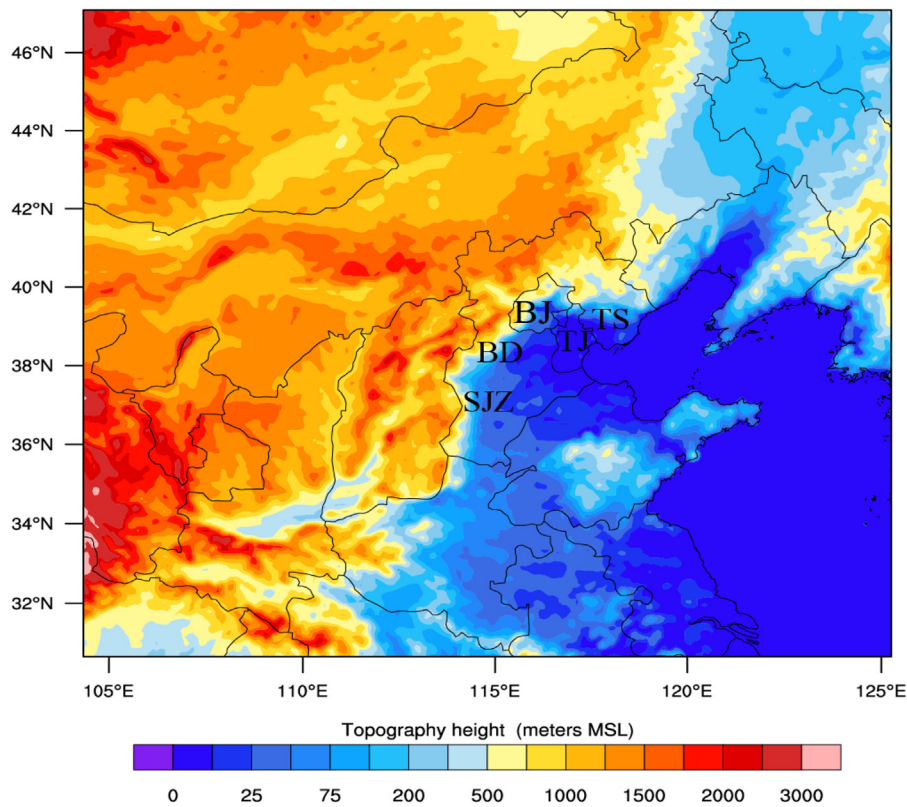


Fig. 1 – Model simulation domain and topography height. BJ: Beijing; TJ: Tianjin; TS: Tangshan; BD: Baoding; SJZ: Shijiazhuang.

Table 1 – Pollutant emission reduction ratios during the red-alert.

Emission region	Source category	SO ₂	NO _x	PM ₁₀	PM _{2.5}	VOC
Beijing	Traffic	–	48%	59%	60%	50%
	Industry	55%	46%	40%	42%	37%
	Other	10%	10%	10%	10%	10%
Tianjin	Traffic	–	–	–	–	–
	Industry	30%	30%	30%	30%	30%
	Other	10%	10%	10%	10%	10%
Hebei	Traffic	–	18%-55%	18%-55%	18%-55%	18%-55%
	Industry	15%-30%	15%-30%	15%-30%	15%-30%	15%-30%
	Other	10%	10%	10%	10%	10%

SO₂: sulfur dioxide; NO_x: nitrogen oxide; PM_{2.5}: the particulate matter less than 2.5 μm; PM₁₀: the particulate matter less than 10 μm; VOC: volatile organic compounds.

aerosol-radiation interaction was turned off. Here, we define the impact of emission reduction on aerosol-radiation interaction as:

$$\Delta_V = \text{base1} - \text{base2} \quad (1)$$

$$\Delta_{V^*} = \text{scenario1} - \text{scenario2} \quad (2)$$

$$\Delta I_V = (\text{base1} - \text{base2}) - (\text{scenario1} - \text{scenario2}) \quad (3)$$

$$\Delta P_V = \Delta I_V / (\text{base1} - \text{scenario1}) \quad (4)$$

where Δ_V represents the effects of aerosol-radiation interaction with reduced anthropogenic emission controls; Δ_{V^*} represents the aerosol-radiation interaction effects without emissions control; ΔI_V represents impact of emission reduction on aerosol-radiation interaction; ΔP_V represents the enhance of emission reduction effects by aerosol-radiation interaction; V represents PM_{2.5} concentration, NO₂ (nitrogen dioxide) concentration, O₃ (ozone) concentration or meteorological variables, such as the surface downward shortwave

radiation (SWDOWN), 2-m temperature (T2), 2-m relative humidity (RH2), and planetary boundary layer height (PBLH).

2. Results and discussion

2.1. Model performance

According to the US EPA model evaluation protocol (US EPA, 2007), the normalized mean bias (NMB), normalized mean gross error (NME) and correlation coefficient (CC) were used for the statistical analysis. The NMB calculation is shown as Eq. (5), the NME calculation is shown as Eq. (6), and the CC calculation is shown as Eq. (7).

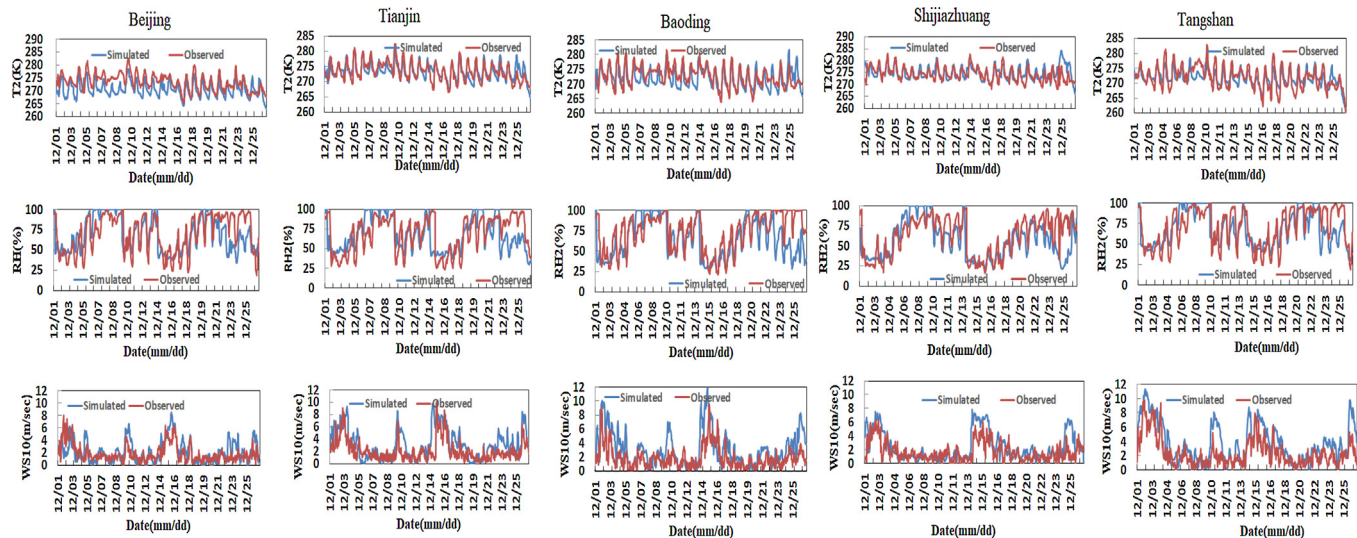
$$\text{NMB} = \frac{1}{N} \sum_{i=1}^N (\text{Sim} - \text{Obs}) / \sum_{i=1}^N \text{Obs} \times 100\% \quad (5)$$

$$\text{NME} = \frac{1}{N} \sum_{i=1}^N |\text{Sim} - \text{Obs}| / \sum_{i=1}^N \text{Obs} \times 100\% \quad (6)$$

Table 2 – Statistical results of simulated and monitored meteorological data.

		Beijing	Tianjin	Baoding	Shijiazhuang	Tangshan
T2 (K)	NMB (%)	-1.00	1.00	-0.34	-0.56	-0.10
	NME (%)	1.00	0.58	0.81	0.98	0.75
	CC	0.72	0.75	0.71	0.53	0.78
RH2 (%)	NMB (%)	-1.98	-1.38	-12.59	-9.23	-3.62
	NME (%)	19.35	23.07	21.22	22.63	18.05
	CC	0.68	0.59	0.64	0.68	0.74
WS10 (m/sec)	NMB (%)	17.90	46.42	67.44	40.59	59.27
	NME (%)	61.70	69.36	69.08	60.63	70.41
	CC	0.57	0.65	0.63	0.63	0.78

NMB: the normalized mean bias; NME: normalized mean gross error; CC: correlation coefficient; T2; temperature at 2 m; RH2: relative humidity at 2 m; WS10: wind speed at 10 m.

**Fig. 2** – Comparison of T2, RH2 and WS10 between the simulated and observed results.

$$CC = \frac{1}{N} \sum_{i=1}^N (\overline{Sim} - \overline{Sim}) \times (\overline{Obs} - \overline{Obs}) / \sqrt{\sum_{i=1}^N (\overline{Sim} - \overline{Sim})^2 \sum_{i=1}^N (\overline{Obs} - \overline{Obs})^2} \quad (7)$$

where Sim is value of the simulation, Obs is value of the observation, \overline{Sim} is average of simulation results, \overline{Obs} is average of observation results, and N is the total number for which the simulations are compared against observations. The unit of CC is same as the unit of the variable calculated, and those of NMB and NME are %.

The hourly air pollutant concentrations were collected by the China National Environmental Monitoring centre (CNEMC). The meteorological data were obtained from the Meteorological Information Comprehensive Analysis and Process System (MICAPS) of the China Meteorological Administration. The evaluation of the base case simulation for surface PM_{2.5} concentrations, NO₂ concentrations, O₃ concentrations, and 2-m temperature (T2), 10-m wind speed (WS10), 2-m relative humidity (RH2) was carried out by comparing the simulated output results with observations provided.

2.1.1. Evaluation of the meteorological variables

Table 2 summarizes the statistics of major meteorological variables for the base scenario simulation and observation for the BTH region in Beijing, Tianjin, Baoding, Shijiazhuang and Tangshan. **Fig. 2** presents the hourly simulated and observed results of T2 (K), RH2 (%), WS10 (m/sec) at typical cities of BTH region. WRF-Chem

simulation results adequately captured the variations of T2 at all sites, with correlation coefficients between 0.53–0.78. The NMB and NME indicated good model performance for T2. The NMB values of T2 were -1%, 1%, 0.34%, -0.56 and -0.1% in Beijing, Tianjin, Baoding, Shijiazhuang and Tangshan, respectively. During this period nearly all sites showed cold biases except for those in Tianjin. The NME values of T2 were between 0.58% and 1%. As shown in **Table 2**, Beijing, Tianjin and Tangshan showed the smallest NMB and NME values for the RH simulation. Baoding and Shijiazhuang presented the relatively large biases for the RH simulation, and they were located in the heavily polluted areas. The RH2 simulation results had correlation coefficients between 0.59 and 0.74. An over-prediction occurred in the hourly WS10 at all the sites, with average bias values between 17.90 and 67.44 in five typical cities. **Fig. 3** shows the hourly simulated and observed results of wind direction. WRF-Chem simulation results adequately captured and reflected the variations of wind direction. The bias of WS10 and Wind direction was caused by the analysis nudging (FDDA) was not applied to the meteorological factors, which suppressed the aerosol-radiation interaction of aerosols on meteorological factors. The simulation results adequately captured the variations in WS10, and all correlation coefficients were greater than 0.5.

2.1.2. Evaluation of air pollutants variables

Table 3 also summarizes the statistics for PM_{2.5}, PM₁₀ (particulate matter less than 10 μm), NO₂ and O₃ concentration in Beijing, Tianjin, Baoding, Shijiazhuang and Tangshan. **Fig. 4** presents the daily simulated and observed results of air pollutants variables in the five typical cities of the BTH region. In Beijing, Tianjin, Baoding,

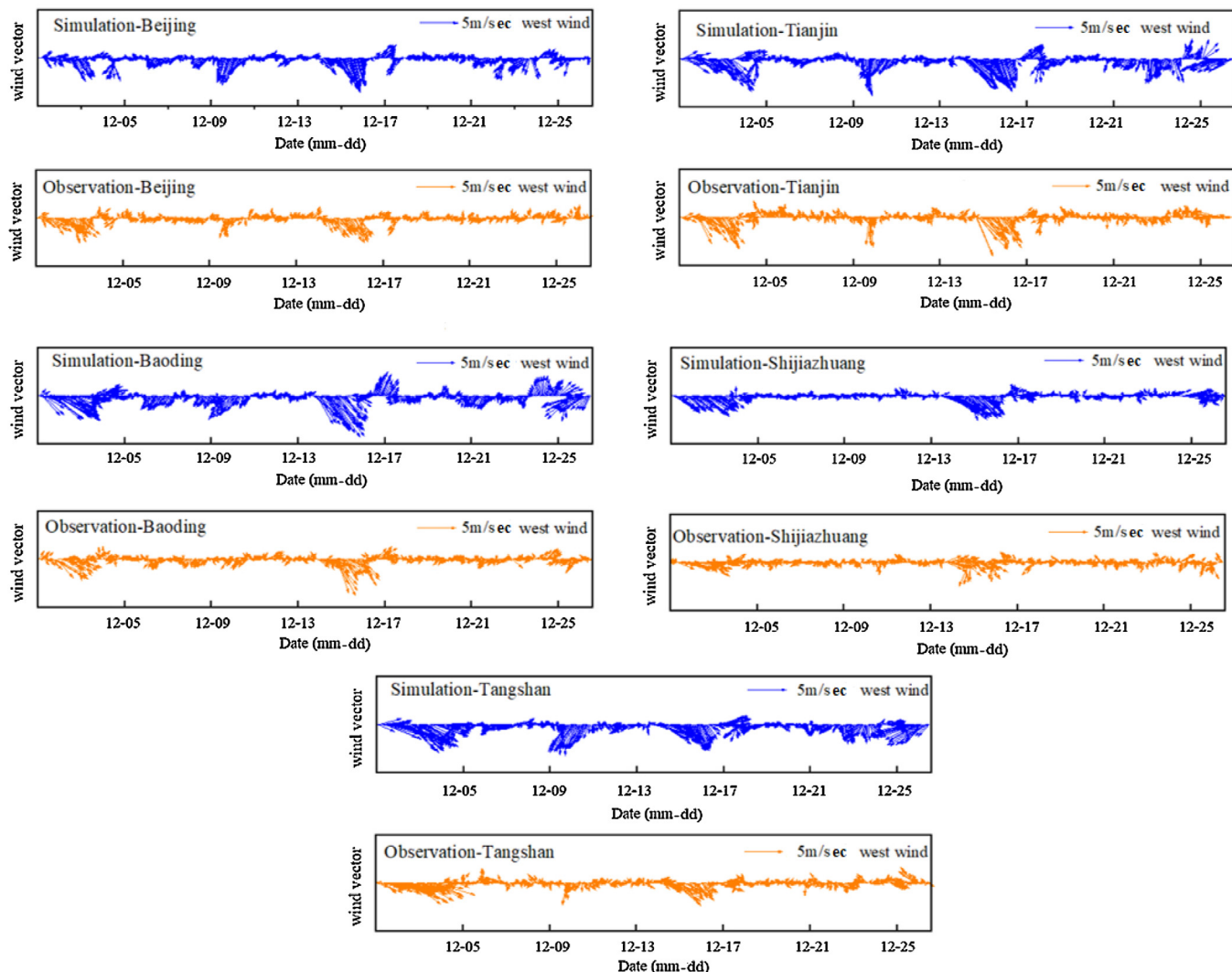


Fig. 3 – Comparison of wind direction between simulated and observed results.

Table 3 – Statistical results of simulated and monitored air pollutant data.

		Beijing	Tianjin	Baoding	Shijiazhuang	Tangshan
$\text{PM}_{2.5}$ ($\mu\text{g}/\text{m}^3$)	NMB (%)	-41.37	24.66	28.35	30.95	-34.79
	NME (%)	43.76	41.66	32.83	35.65	36.82
	CC	0.67	0.58	0.80	0.74	0.80
PM_{10} ($\mu\text{g}/\text{m}^3$)	NMB (%)	-33.89	-31.88	-24.80	-40.42	-39.88
	NME (%)	50.04	37.83	42.55	42.02	41.03
	CC	0.58	0.78	0.61	0.79	0.80
NO_2 ($\mu\text{g}/\text{m}^3$)	NMB (%)	7.72	12.98	15.71	1.33	11.00
	NME (%)	23.47	29.32	24.45	32.70	22.66
	CC	0.7	0.57	0.81	0.77	0.76
O_3 ($\mu\text{g}/\text{m}^3$)	NMB (%)	-10.86	3.5	5.70	5.10	12.71
	NME (%)	33.23	51.35	48.09	43.24	48.01
	CC	0.79	0.71	0.77	0.92	0.66

Shijiazhuang and Tangshan, the NMB values for the comparison results of $\text{PM}_{2.5}$ were -41.37%, 24.66%, 28.35%, 30.95%, and -34.79%, respectively; the NMB values for the comparison results of PM_{10} were -33.89%, -31.88%, -24.80%, -40.42%, and -39.88%, respectively; the NMB values for NO_2 were 7.72%, 12.98%, 15.71%, 1.33%, and 11.00%, respectively; and the NMB values for O_3 were -10.86%, 3.5%, 5.70%, 5.10%, and 12.71%, respectively. The NME values from the simulation were generally between 22.66% and 51.35%. The bias might be from the following: the emission inventories could

be highly uncertain at individual sites, which would affect the accuracy of simulation results; additionally, the uncertainties associated with the meteorology simulation could affect the results. The relatively large biases of $\text{PM}_{2.5}$ concentration during heavily polluted days were relevant with the underestimated RH2, which was not favorable for $\text{PM}_{2.5}$ particles accumulation. At the same time, inherent characteristics of the model can produce a large bias during heavily polluted days (Wang et al., 2013). Overall, in this work, WRF-Chem predicts variables reasonably well. The

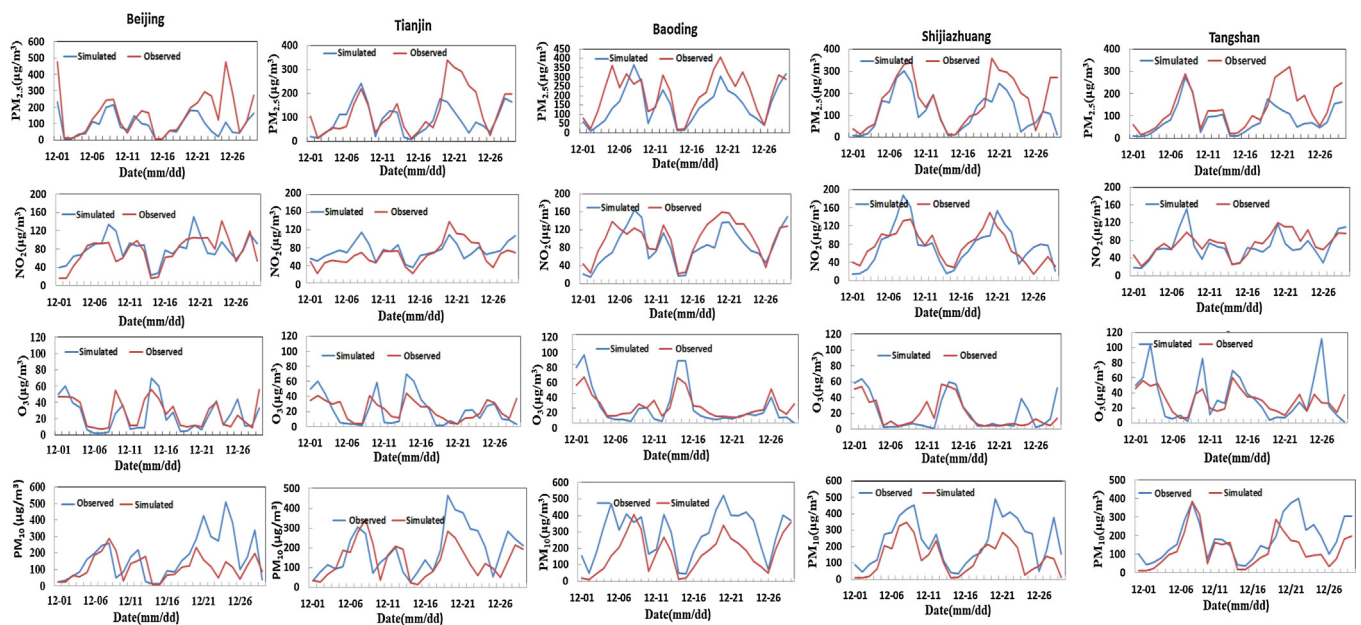


Fig. 4 – Comparison of air quality concentrations between simulated and observed results.

correlation coefficients of the air pollutant concentrations between the simulated and observed were between 0.57 and 0.92. The model simulation results shown as Fig. 4 can clearly represent the air pollution process. All parameters followed the guidelines of the US Environmental Protection Agency (2007).

2.2. Impact of emission reduction on aerosol-radiation interaction

2.2.1. Impacts on meteorological variables

Fig. 5 shows the spatial distributions of mean air quality concentration (PM_{2.5}, PM₁₀, NO₂, O₃) in the BTH region over the simulation period. Fig. 6 shows the mean distributions of the meteorological variables (SWDOWN, T2, RH2, PBLH) in the entire simulation period over the region. Heavy pollutions formed in the southern part and spread towards the northern parts of the region. The air pollution accumulated in front of Yanshan and Taihang Mountains in the west and north of the BTH region. Shijiazhuang, Baoding, Beijing and most other BTH region had heavy air pollution.

Four model sensitivity results were compared to examine the aerosol-radiation interaction effects on meteorological variables, whose spatial distributions are also shown in Fig. 7. The monthly mean aerosol-radiation interaction effects in five typical cities over BTH region are provided in Table 4.

The aerosol-radiation interaction decreased the downward surface shortwave radiation (Δ_{SWDOWN}) by 0–28 W/m² over the simulation domain, particularly in areas with severe PM_{2.5} pollution. The spatial mean contributions of the aerosol-radiation interaction with emission reduction to downward shortwave radiation (Δ_{SWDOWN}) averaged over the simulation period were about 14.83, 14.48, 18.53, 16.19 and 12.26 W/m² decreases in Beijing, Tianjin, Baoding, Shijiazhuang and Tangshan, respectively. T2 was reduced by up to 0.3–1.5°C (Δ_{T2}) in the southern BTH region. This cooling effect occurred over most parts of the domain. This result is because aerosol reduce incoming solar radiation via scattering and absorption, therefore decreasing surface/near surface temperatures. The monthly average RH2 exhibited an obvious increase in the middle and southern parts of the BTH region. The mean spatial contributions of the aerosol-radiation interaction to the RH2 (Δ_{RH2}) over the simulation period were

Table 4 – Impacts on meteorological variables in typical cities over simulation period.

	Δ_V	Δ_{V^*}	Δ_{IV}	Δ_{IV}/Δ_V
Beijing				
T2 (K)	−0.69	−0.74	0.04	−6%
PBLH (m)	−19.47	−20.93	1.46	−8%
SWDOWN (W/m ²)	−14.83	−16.72	1.89	−13%
RH2 (%)	1.93	2.02	−0.09	−5%
Tianjin				
T2 (K)	−0.63	−0.67	0.04	−7%
PBLH (m)	−22.32	−22.97	0.65	−3%
SWDOWN (W/m ²)	−14.48	−16.33	1.85	−13%
RH2 (%)	3.61	3.73	−0.12	−3%
Baoding				
T2 (K)	−0.72	−0.77	0.05	−6%
PBLH (m)	−28.23	−29.59	1.36	−5%
SWDOWN (W/m ²)	−18.53	−20.88	2.36	−13%
RH2 (%)	3.67	3.87	−0.20	−5%
Shijiazhuang				
T2 (K)	−0.55	−0.56	0.01	−2%
PBLH (m)	−23.78	−29.92	6.14	−26%
SWDOWN (W/m ²)	−16.19	−18.37	2.18	−13%
RH2 (%)	2.81	2.88	−0.07	−2%
Tangshan				
T2 (K)	−0.44	−0.45	0.01	−2%
PBLH (m)	−19.11	−19.27	0.16	−1%
SWDOWN (W/m ²)	−12.26	−13.73	1.47	−12%
RH2 (%)	2.22	2.29	−0.07	−3%

Δ_V : the effects of aerosol-radiation interaction with reduced anthropogenic emission controls; Δ_{V^*} : the aerosol-radiation interaction effects without emissions control; Δ_{IV} : impact of emission reduction on aerosol-radiation interaction.

approximately 1.93%, 3.61%, 3.67%, 2.81%, and 2.22% in Beijing, Tianjin, Baoding, Shijiazhuang, and Tangshan, respectively. The aerosol-radiation interaction reduced the PBLH (Δ_{PBLH}) in most area of the BTH region by 5–30 m. The mean spatial contribution of the aerosol-radiation interaction to the PBLH (Δ_{PBLH}) over the simulation period was between 6.56% and 10.3% decrease in five typical cities in the BTH region. In the eastern continental United States, aerosol direct feedback decreased the downward shortwave radiation by 11.3 W/m², the T2 by 0.16 K, and the PBLH by 22.4 m in winter (Zhang et al., 2010). In east China the monthly-mean

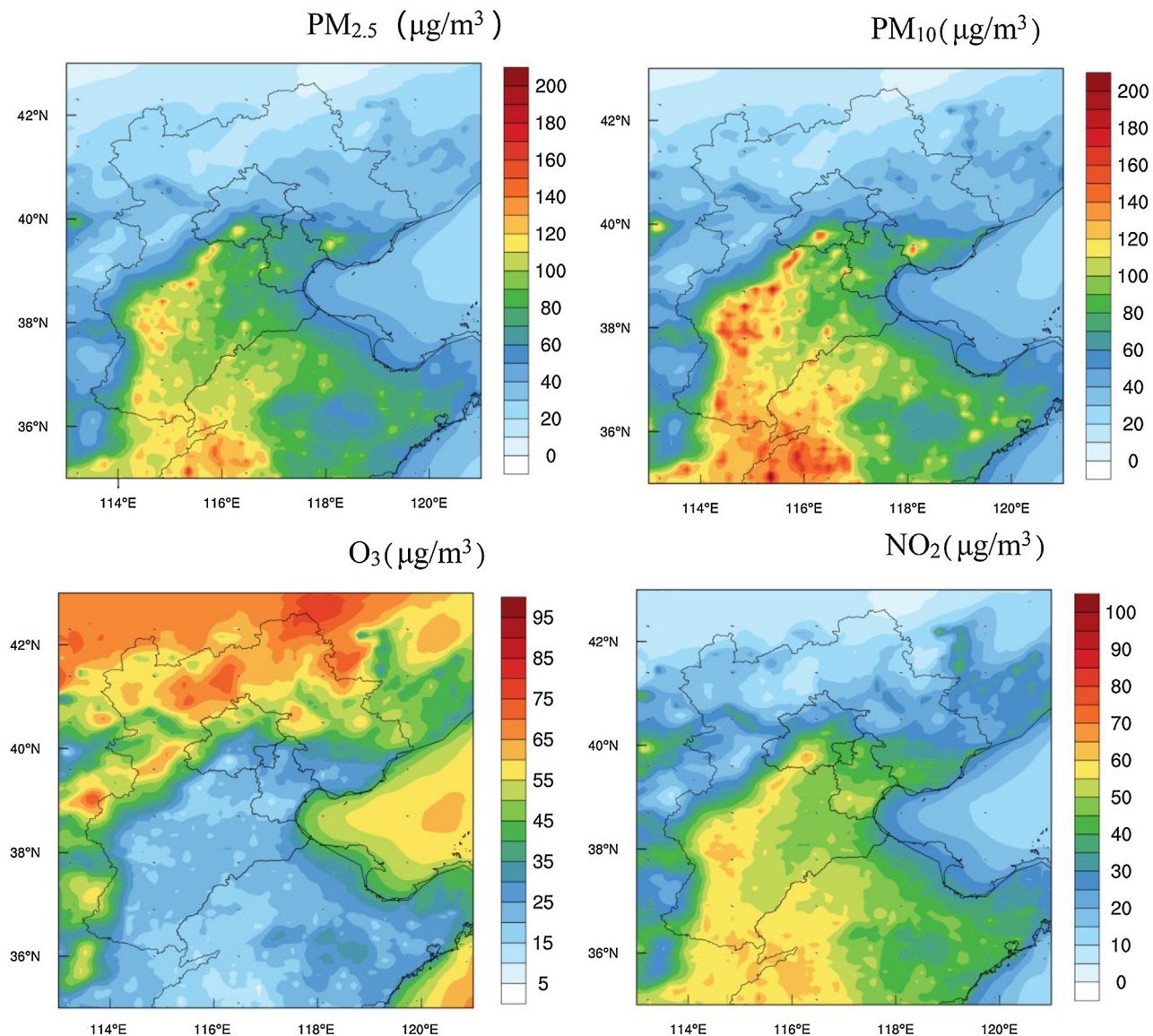


Fig. 5 – Spatial distributions of mean air quality concentration from the base1 simulation.

SWDOWN, T2 and PBLH can be decreased by -12.37 W/m², -0.24°C and -31.59 m by aerosol-radiation interaction in October (Chen et al., 2015). The results in the BTH region in this paper were similar to those previous studies.

Fig. 7 also shows the mean spatial distributions of ΔI_{SWDOWN} , ΔI_{T2} , ΔI_{RH2} , and ΔI_{PBLH} , and the weakened aerosol-radiation interaction effect caused by emission reductions is evident. During the simulation period, the interaction effect due to emission reductions increased the downward shortwave radiation (ΔI_{SWDOWN}) by an average of 0–5 W/m² (~15%, $\Delta I_{\text{SWDOWN}}/\Delta_{\text{SWDOWN}}$) in the BTH region, leading to an increase in the surface temperature (ΔI_{T2}) of 0–0.05°C (~7%, $\Delta I_{\text{T2}}/\Delta_{\text{T2}}$), an increase in the daytime mean PBLH (ΔI_{PBLH}) of 0–8 m (~28%, $\Delta I_{\text{PBLH}}/\Delta_{\text{PBLH}}$), and a weaker decrease in the daytime mean 2 m RH (ΔI_{RH}) of 0.5% (~5%, $\Delta I_{\text{RH}}/\Delta_{\text{RH}}$). The impact of aerosol-radiation interaction effects on surface aerosols changed the meteorological variables, making the atmosphere more stable and favorable for pollution accumulation. Emission reductions lead to weaker impacts of aerosol-radiation interaction effects on meteorology. Larger impacts caused by the weakened aerosol-radiation interaction effects can be seen over regions with higher pollution.

2.2.2. Impacts on air quality

Fig. 8 shows the mean spatial distributions of aerosol-radiation interaction effects on the air quality concentrations (PM_{2.5}, PM₁₀, NO₂, O₃) in the BTH region during the simulation period. The effect on the PM_{2.5} and PM₁₀ concentrations showed negative correlations with the SWDOWN, T2 and PBLH. These results indicated the remarkable decrease in the downward shortwave radiation at the surface caused by the aerosol-radiation interaction reduced the ground surface temperature and caused more stable lower atmosphere (i.e., the increased in RH2 and reduction in PBL height). As a result, the stable meteorological conditions suppressed dispersion of air pollutants and increased the ground PM_{2.5} and PM₁₀ concentrations. The aerosol-radiation interaction led to a strong increase in PM_{2.5} concentration in the middle and southern parts of Hebei Province, where the aerosol anthropogenic emissions are strong. The contributions of aerosol-radiation interaction with emission control increased the PM_{2.5} concentration ($\Delta_{\text{PM2.5}}$) by 1.75, 2.00, 2.10, 1.90, and 3.63 $\mu\text{g}/\text{m}^3$ in Beijing, Tianjin, Baoding, Shijiazhuang, and Tangshan, respectively, as shown in Table 5. The aerosol-radiation interaction effect increased the PM₁₀ concentration (Δ_{PM10}) by 2.20, 2.46, 2.71, 1.56, and 4.35 $\mu\text{g}/\text{m}^3$ in

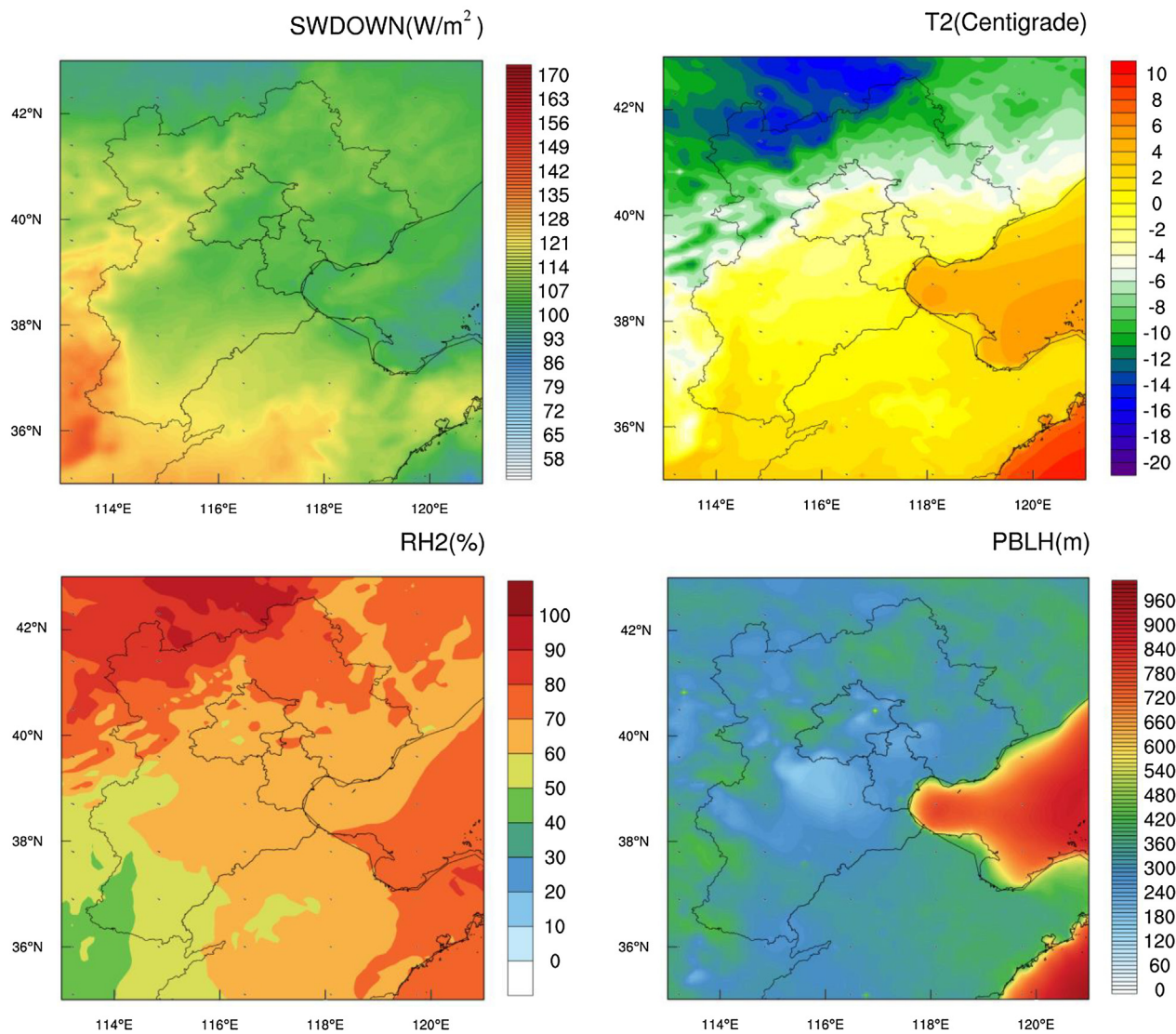


Fig. 6 – Mean distributions of meteorological variables from the base1 simulation. SWDOWN: downward shortwave radiation; PBLH: planetary boundary layer height.

Beijing, Tianjin, Baoding, Shijiazhuang, and Tangshan, respectively. The aerosol-radiation interaction increased the NO_2 concentration in most BTH regions except the northeast region. In most areas of the region, NO_2 increased by 0–4.5 $\mu\text{g}/\text{m}^3$. The highest values can be seen in the heavily polluted areas. The concentration of O_3 at surface decreased by 0–1.55 $\mu\text{g}/\text{m}^3$ in most areas of the five typical cities. Many studies indicated that high temperature, low relative humidity and high shortwave radiation are related to high concentrations of O_3 at surface (Nair et al., 2002; Duenas et al., 2002). During the simulation period, the T2 and SWDOWN decreased, and the RH2 increased due to the aerosol-radiation interaction. These changes in meteorological conditions decreased the regional mean O_3 concentration.

Table 5 also shows that the $\Delta I_V/\Delta P_V$ was defined for quantifying the effectiveness of emission control measures in the model simulation with considered aerosol-radiation interaction. The emergency control measures implemented in the BTH region were effective in reducing air pollution. The $\text{PM}_{2.5}$ concentration decreased by 20–40 $\mu\text{g}/\text{m}^3$ in most BTH regions, with decreases of 23.14%, 25.33%, 31.55%, 25.40%, and 22.87% in Beijing, Tianjin, Baoding, Shijiazhuang and Tangshan, respectively. PM_{10} had a similar trend to $\text{PM}_{2.5}$, with decreases of 28.10%–38.99% in the five typical cities. The results conformed to the pollutant emission

reduction ratios in the BTH region during the red alert period in December 2015 (Jia et al., 2017). The NO_2 concentrations decreased by 9.57–17.86 $\mu\text{g}/\text{m}^3$ in the region. However, the O_3 concentration increased. This phenomenon of increasing O_3 concentrations during emission reduced period was also found in previous studies (Wen et al., 2016). This reason of the result might be as follows: the complex effects of O_3 reaction; the reducing ratio between NO_x and VOCs (Volatile organic compounds) was not considered in the emission control measures; the decreased of T2 and SWDOWN caused by aerosol-radiation feedbacks were unfavorable for high O_3 concentration.

Fig. 8 also shows how the air pollution concentrations over the BTH region would change if emission reductions were applied with or without aerosol-radiation interaction considered. The air pollution concentrations ($\Delta I_{\text{PM}2.5}$, $\Delta I_{\text{PM}10}$, ΔI_{NO_2} , and ΔI_{O_3}) were enhanced by 0.16–1.74, 0.26–2.04, 0.18–1.65, and 0.03–0.19 $\mu\text{g}/\text{m}^3$ in Beijing, Tianjin, Baoding, Shijiazhuang, and Tangshan, respectively. We can see that if there were aerosol-radiation interactions, the impacts of emission reductions were distinctly enhanced. It also proved that under the heavy pollution conditions, the aerosol-radiation interaction effects were more obvious. The $\Delta P_{\text{PM}2.5}$, $\Delta P_{\text{PM}10}$, ΔP_{NO_2} for the BTH region during the simulation period reaches 7.62%, 6.90%, and 11.62%, respectively, indicating a sig-

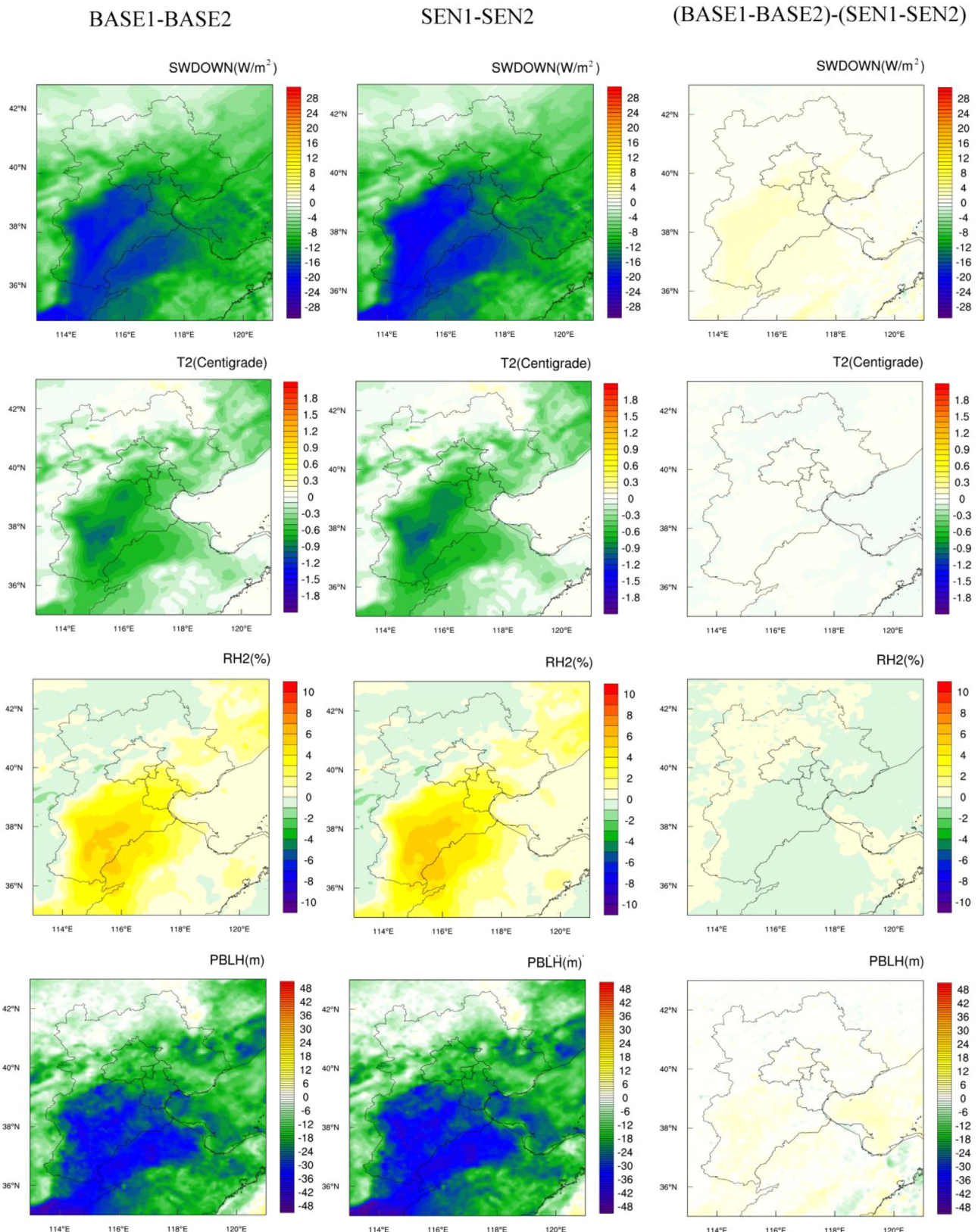


Fig. 7 – Simulated results of aerosol-radiation interaction on regional meteorological factors. BASE1-BASE2: the effects of aerosol-radiation interaction with reduced anthropogenic emission controls; SEN1-SEN2: the aerosol-radiation interaction effects without emissions control; (BASE1-BASE2)-(SEN1-SEN2): impact of emission reduction on aerosol-radiation interaction.

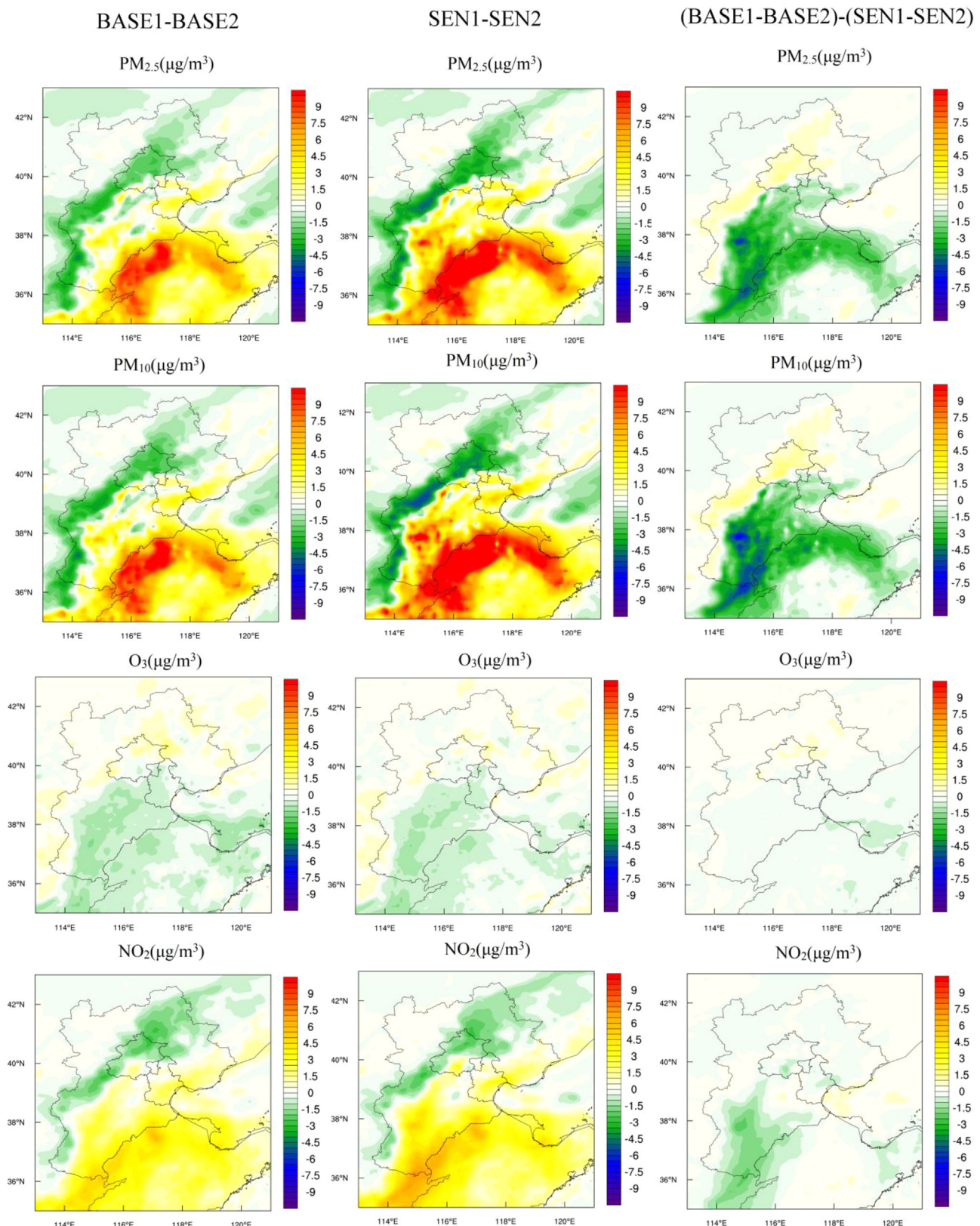
**Fig. 8 –** Simulated results of aerosol-radiation interaction on regional air quality.

Table 5 Impacts on air quality in typical cities over simulation period.

	ΔV	ΔV^*	ΔI_V	ΔP_V
Beijing				
PM _{2.5} ($\mu\text{g}/\text{m}^3$)	1.75	2.20	-0.45	1.96%
PM ₁₀ ($\mu\text{g}/\text{m}^3$)	2.20	2.93	-0.73	2.59%
NO ₂ ($\mu\text{g}/\text{m}^3$)	1.43	2.23	-0.80	4.49%
O ₃ ($\mu\text{g}/\text{m}^3$)	-0.83	-0.64	-0.19	-1.45%
Tianjin				
PM _{2.5} ($\mu\text{g}/\text{m}^3$)	2.00	3.51	-1.51	5.97%
PM ₁₀ ($\mu\text{g}/\text{m}^3$)	2.46	4.33	-1.87	5.64%
NO ₂ ($\mu\text{g}/\text{m}^3$)	1.43	1.61	-0.18	1.83%
O ₃ ($\mu\text{g}/\text{m}^3$)	-1.55	-1.52	-0.03	-0.39%
Baoding				
PM _{2.5} ($\mu\text{g}/\text{m}^3$)	2.10	3.10	-1.00	3.17%
PM ₁₀ ($\mu\text{g}/\text{m}^3$)	2.71	4.31	-1.60	4.09%
NO ₂ ($\mu\text{g}/\text{m}^3$)	2.76	4.41	-1.65	10.72%
O ₃ ($\mu\text{g}/\text{m}^3$)	-1.44	-1.36	-0.08	-2.07%
Shijiazhuang				
PM _{2.5} ($\mu\text{g}/\text{m}^3$)	1.90	2.06	-0.16	0.64%
PM ₁₀ ($\mu\text{g}/\text{m}^3$)	1.56	1.83	-0.26	0.79%
NO ₂ ($\mu\text{g}/\text{m}^3$)	0.01	0.53	-0.53	4.20%
O ₃ ($\mu\text{g}/\text{m}^3$)	-0.27	-0.16	-0.11	-6.23%
Tangshan				
PM _{2.5} ($\mu\text{g}/\text{m}^3$)	3.63	5.37	-1.74	7.62%
PM ₁₀ ($\mu\text{g}/\text{m}^3$)	4.35	6.39	-2.04	6.90%
NO ₂ ($\mu\text{g}/\text{m}^3$)	3.22	4.33	-1.11	11.62%
O ₃ ($\mu\text{g}/\text{m}^3$)	-1.14	-1.10	-0.04	-0.46%

nificant percentage of underestimated air pollution concentration reduction due to emission control measures in a model simulation without aerosol-radiation interaction considered. The results were similar to those in Zhou et al. (2019), which found surface PM_{2.5} concentration decrease in Beijing due to emission reductions can be 6.7%–21.9% larger than that estimated without aerosol-radiation interaction. The relationship between the aerosol-radiation interaction effects and air quality concentrations can have an important implication for assessing the effectiveness of emission control measures.

3. Conclusions

In this study, WRF-Chem model was applied to evaluate the impact of emission reduction on aerosol-radiation interaction during heavy pollution periods over the Beijing-Tianjin-Hebei region in China. Four tests were conducted, including the simulation with/without emission reduction and aerosol-radiation interaction turned on/off. The simulation results of air pollutant concentrations and meteorological variables were verified. An acceptable agreement between the simulated and observed concentrations was achieved.

In summary, we investigated the impact of aerosol-radiation interaction effects on changes in meteorological variables, which made the atmosphere more stable and favorable for pollution accumulation. If there were aerosol-radiation interactions in the simulation, the downward shortwave radiation at the surface decreased, leading to decrease in temperature. As a result, it suppressed the development of PBLH and increased the relative humidity. Emission reductions caused impacts of aerosol-radiation interaction effects on meteorology variables. During the simulation period, the interaction effect due to emission reductions increased the downward shortwave radiation by an average of 0–5 W/m², leading to an increase in surface temperature of 0–0.05°C, increase in the daytime mean PBLH of 0–8 m, and decrease in the daytime mean RH2 of 0.5%.

The effectiveness of emission control measures in model simulation with and without consideration of aerosol-radiation interaction was estimated. With aerosol-radiation interactions,

PM_{2.5} concentration decreased by 20–40 $\mu\text{g}/\text{m}^3$ in most BTH regions. The PM₁₀ decreased by 28.10%–38.99%. We also found that if there were aerosol-radiation interactions, the impacts of emission reductions were distinctly enhanced. The enhancement of PM_{2.5}, PM₁₀, and NO₂ emission reduction effects reaches 7.62%, 6.90%, and 11.62%, respectively, over the region.

The relationships between aerosol-radiation interaction effects and air quality concentrations can have an important implication for assessing the effectiveness of emission control measures. However, the uncertainties that might affect the simulated model results in this study were as follows: aerosols could further affect cloud and precipitation conditions, and the influences of aerosol cloud effect were not considered in the model. Future work is needed to better represent the model aerosol-radiation interaction associated with aerosol cloud effect, and assess their impacts on emission reductions.

Declaration of competing interest

The authors declare that they have no known competing financial interests or personal relationships that could have appeared to influence the work reported in this paper.

Acknowledgments

This research was supported by the National Key Research and Development Program of China (Nos. 2016YFC0208905, 2017YFC1501406, and 2017YFC0210300), the National Natural Science Foundation of China (Nos. 51808549, 21806183 and 51774038), Beijing Major Science and Technology Project (No. Z181100005418014), and Chinese Academy of Meteorological Sciences Foundation (No. 2018Y001).

References

- Boucher, O., Randall, D., Artaxo, P., Bretherton, C., Feingold, G., Forster, P., et al., 2013. Clouds and aerosols. In: Stocker, T.F., Qin, D., Plattner, G., Tignor, M., Allen, S.K., Boschung, J., et al. (Eds.), Climate Change 2013: The Physical Science Basis. Contribution of Working Group I to the Fifth Assessment Report of the Intergovernmental Panel On Climate Change. Cambridge University Press, Cambridge, UK and New York, NY, USA.
- Cao, J.J., Xu, H.M., Xu, Q., Chen, B.H., Kan, H.D., 2012. Fine particulate matter constituents and cardiopulmonary mortality in a heavily polluted Chinese city. Environ. Health Perspect. 120, 373–378.
- Charlson, R.J., Schwartz, S.E., Hales, J.M., Cess, R.D., Coakley, J.A., Hansen, J.E., et al., 1992. Climate forcing by anthropogenic aerosols. Science 255, 423–430.
- Chen, D.S., Ma, X., Xie, X., Wei, P., Wen, W., Xu, T.T., et al., 2015. Modelling the effect of aerosol feedbacks on the regional meteorology factors over China. Aerosol Air Qual. Res. 15, 1559–1579.
- Chou, M.D., Suarez, M.J., 1994. An efficient thermal infrared radiation parameterization for use in general circulation models. NASA Technical Memorandum, 3. NASA Goddard Space Flight Center, Greenbelt, MD, United States, pp. 1–85 104606.
- Dhar, P., De, B.K., Banik, T., Gogoi, M.M., Babu, S.S., Guha, A., 2017. Atmospheric aerosol radiative forcing over a semi-continental location Tripura in North-East India: Model results and ground observations. Sci. Total Environ. 580, 499–508.
- Dong, C., Matsui, H., Spak, S., Kalafut-Pettibone, A., Stanier, C., 2018. Impacts of new particle formation on short-term meteorology and air quality as determined by the NPF-explicit WRF-chem in the midwestern United States. Atmos. Chem. Phys. 19 (2), 204.
- Duenas, C., Fernandez, M.C., Canete, S., Carretero, J., Liger, E., 2002. Assessment of ozone variations and meteorological effects in an urban area in the Mediterranean coast. Sci. Total Environ. 299, 97–113.
- Fast, J.D., Gustafson, W.I., Easter, R.C., Zaveri, R.A., Barnard, J.C., Chapman, E.G., et al., 2006. Evolution of ozone, particulates, and aerosol direct radiative forcing in the vicinity of Houston using a fully coupled meteorology–chemistry–aerosol model. J. Geophys. Res. 111 (D21), D21305.
- Forkel, R., Werhahn, J., Hansen, A.B., McKeen, S., Peckham, S., Grell, G., et al., 2012. Effect of aerosol radiation feedback on regional air quality - a case study with WRF/Chem. Atmos. Environ. 53, 202–211.
- Gao, M., Carmichael, G.R., Wang, Y.S., Saide, P.E., Yu, M., Xin, J.Y., et al., 2016. Modeling study of the 2010 regional haze event in the North China Plain. Atmos. Chem. Phys. 16 (3), 1673–1691.
- Gao, Y., Zhao, C., Liu, X.H., Zhang, M.G., Leung, R., 2014. WRF-Chem simulations of aerosols and anthropogenic aerosol radiative forcing in East Asia. Atmos. Environ. 92, 250–266.

- Goto, D., Kikuchi, M., Suzuki, K., 2019. Aerosol model evaluation using two geostationary satellites over East Asia in May 2016. *Atmos. Res.* 217, 93–113.
- Guo, J., Liu, H., Wang, F., Huang, J.F., Xia, F., Lou, M.Y., et al., 2016. Three-dimensional structure of aerosol in China: A perspective from multi-satellite observations. *Atmos. Res.* 178–179, 580–589.
- He, H., Tie, X.X., Zhang, Q., Liu, X.E., Gao, Q., Li, X., et al., 2015. Analysis of the causes of heavy aerosol pollution in Beijing, China: A case study with the WRF-Chem model. *Particuology* 20, 32–40.
- Hirti, M., Stuefer, M., Arnold, D., 2019. The effects of simulating volcanic aerosol radiative feedbacks with WRF-Chem during the Eyjafjallajökull eruption, April and May 2010. *Atmos. Environ.* 198, 194–206.
- Hong, S.Y., Noh, Y., Dudhia, J., 2006. A new vertical diffusion package with an explicit treatment of entrainment processes. *Mon. Wea. Rev.* 134, 2318–2341.
- Leng, C.P., Duan, J.Y., Chen, X., Zhang, H.F., Wang, Y.F., Wang, Y.Y., et al., 2016. Insights into a historic severe haze event in Shanghai: synoptic situation, boundary layer and pollutants. *Atmos. Chem. Phys.* 16 (14), 9221–9234.
- Li, J., Han, Z., 2016. A modeling study of severe winter haze events in Beijing and its neighboring regions. *Atmos. Res.* 170, 87–97.
- Jia, J., Cheng, S.Y., Liu, L., Lang, J.L., Wang, G., Chen, G.L., et al., 2017. An integrated wrf-camx modeling approach for impact analysis of implementing the emergency PM_{2.5} control measures during Red Alerts in Beijing in December 2015. *Aerosol Air Qual. Res.* 17, 2491–2508.
- Kalenderski, S., Stenchikov, G., 2016. High-resolution regional modeling of summertime transport and impact of African dust over the Red Sea and Arabian Peninsula. *J. Geophys. Res. Atmos.* 121 (11), 6435–6458.
- Canaya, Y., Matsui, H., Taketani, F., Tketani, F., Pan, X.L., Komazaki, Y., et al., 2017. Observed and modeled mass concentrations of organic aerosols and PM_{2.5} at three remote sites around the east china sea: roles of chemical aging. *Aerosol Air Qual. Res.* 17, 3091–3105.
- Kang, N., Kumar, K.R., Hu, K., Yu, X.N., Yin, Y., 2016. Long-term (2002–2014) evolution and trend in Collection 5.1 Level-2 aerosol products derived from the MODIS and MISR sensors over the Chinese Yangtze River Delta. *Atmos. Res.* 181, 29–43.
- Lang, J.L., Zhang, Y.Y., Zhou, Y., Cheng, S.Y., Chen, D.S., Guo, X.R., et al., 2017. Trends of PM_{2.5} and chemical composition in Beijing, 2000–2015. *Aerosol Air Qual. Res.* 17 (2), 412–425.
- Ma, Y., Xin, J.Y., Zhang, W.Y., Liu, Z.R., Ma, Y.J., Kong, L.B., et al., 2019. Long-term variations of the PM_{2.5} concentration identified by MODIS in the tropical rain forest, Southeast Asia. *Atmos. Res.* 219, 140–152.
- Makar, P.A., Gong, W., Milbrandt, J., 2015. Feedbacks between air pollution and weather, Part 1: Effects on weather. *Atmos. Environ.* 115, 442–469.
- Mlawer, E.J., Taubman, S.J., Brown, P.D., Iacono, M.J., Clough, S.A., 1997. Radiative transfer for inhomogeneous atmospheres: RRTM, a validated correlated-k model for the longwave. *J. Geophys. Res.* 102 (16), 16,663–16,682 663–16,682.
- Nair, R., Chand, D., Lal, S., Modh, K.S., Naja, M., Parameswaran, K., et al., 2002. Temporal variations in surface ozone at Thumba (8.6°N, 77°E)- a tropical coastal site in India. *Atmos. Environ.* 36, 603–610.
- Obregón, M.A., Costa, M.J., Silva, A.M., Serrano, A., 2018. Impact of aerosol and water vapour on SW radiation at the surface: Sensitivity study and applications. *Atmos. Res.* 213, 252–263.
- Pere, J.C., Mallet, M., Pont, V., Bessagnet, B., 2011. Impact of aerosol direct radiative forcing on the radiative budget, surface heat fluxes, and atmospheric dynamics during the heat wave of summer 2003 over western Europe: A modeling study. *J. Geophys. Res. Atmos.* 116, D23119 D23119.
- Rizza, U., Miglietta, M.M., Mangia, C., 2018. Sensitivity of WRF-Chem model to land surface schemes: Assessment in a severe dust outbreak episode in the Central Mediterranean (Apulia Region). *Atmos. Res.* 201, 168–180.
- Santos, D., Costa, M.J., Silva, A.M., 2008. Direct SW aerosol radiative forcing over Portugal. *Atmos. Chem. Phys.* 8, 5771–5786.
- Sharma, R., Balasubramanian, R., 2018. Size-fractionated particulate matter in indoor and outdoor environments during the 2015 haze in Singapore: potential human health risk assessment. *Aerosol Air Qual. Res.* 18, 904–917.
- Sun, Y., Wang, Z.F., Wild, O., Xu, W., Chen, C., Fu, P.Q., et al., 2016. APEC Blue": secondary aerosol reductions from emission controls in Beijing. *Sci. Rep.* 6, 20668.
- Thompson, G., Field, P.R., Rasmussen, R.M., Hall, W.D., 2008. Explicit forecasts of winter precipitation using an improved bulk microphysics scheme. Part II: Implementation of a new snow parameterization. *Mon. Wea. Rev.* 136, 5095–5115.
- Toll, V., Männik, A., 2015. The direct radiative effect of wildfire smoke on a severe thunderstorm event in the Baltic Sea region. *Atmos. Res.* 155, 87–101.
- US EPA (Environmental Protection Agency), 2007. Guidance on the Use of Models and Other Analyses for Demonstrating Attainment of Air Quality Goals for Ozone, PM2.5, and Regional Haze. Available: <https://www3.epa.gov/scram001/guidance/guide/draft-final-03.pdf>. Accessed May 4, 2019.
- Wang, L.T., Wei, Z.M., Yang, J.Z., Zhang, Y., Zhang, F.F., Su, J., et al., 2013. The 2013 severe haze over southern Hebei, China: model evaluation, source apportionment, and policy implications. *Atmos. Chem. Phys.* 13 (11), 28395–28451.
- Wang, L.T., Fu, J.S., Wei, W., Meng, C.C., Ma, S.M., Wang, J.D., 2018. How aerosol-radiation interaction influence the source contributions to PM_{2.5} concentrations over Southern Hebei. China Severe Winter Haze Episodes. *Front. Environ. Sci. Eng.* 12, 3.
- Wang, G., Cheng, S.Y., Lang, J.L., Yang, X.W., Wang, X.Q., Chen, G.L., et al., 2017. Characteristics of PM_{2.5} and assessing effects of emission- Reduction measures in the heavy polluted city of Shijiazhuang, before, during, and after the Ceremonial Parade 2015. *Aerosol Air Qual. Res.* 17, 499–512.
- Wang, T., Nie, W., Gao, J., Xue, L.K., Gao, X.M., Wang, X.F., et al., 2010. Air quality during the 2008 Beijing Olympics: secondary pollutants and regional impact. *Atmos. Chem. Phys.* 10, 7603–7615.
- Wen, W., Cheng, S.Y., Chen, X.F., Wang, G., Li, S., Wang, X.Q., et al., 2016. Impact of emission control on PM_{2.5} and the chemical composition change in Beijing-Tianjin-Hebei during the APEC summit 2014. *Environ. Sci. Pollut. Res.* 105, 432–436.
- Xing, J., Mathur, R., Pleim, J., Hogrefe, C., Gan, C.M., Wong, D.C., et al., 2015. Air pollution and climate response to aerosol direct radiative effects: A modeling study of decadal trends across the northern hemisphere. *J. Geophys. Res. Atmos.* 120, 12221–12236.
- Xu, W.Q., Sun, Y.L., Chen, C., Du, W., Han, T.T., Wang, Q.Q., et al., 2015. Aerosol composition, oxidation properties, and sources in Beijing: results from the 2014 Asia-Pacific Economic Cooperation summit study. *Atmos. Chem. Phys.* 15, 13681–13698.
- Zaveri, R.A., Peters, L.K., 1999. A new lumped structure photochemical mechanism for large-scale applications. *J. Geophys. Res.* 104 (D23), 30387–30415.
- Zaveri, R.A., Easter, R.C., Fast, J.D., Peters, L.K., 2008. Model for simulating aerosol interactions and chemistry (MOSAIC). *J. Geophys. Res.* 113 (D13), D13204.
- Zhang, X.Y., Wang, Y.Q., Lin, W.L., Zhang, Y.M., Zhang, X.C., Gong, S., et al., 2009. Changes of atmospheric composition and optical properties over Beijing 2008 Olympic monitoring Campaign. *Bull. Am. Meteorol. Soc.* 90, 1633–1651.
- Zhang, Y., Wen, X.Y., Jang, C.J., 2010. Simulating Chemistry-aerosol-cloud-radiation-climate Feedbacks over the Continental U.S. using the online-coupled weather research recasting model with chemistry (WRF/Chem). *Atmos. Environ.* 44, 3568–3582.
- Zhang, Z., Zhang, X., Gong, D., Kim, S.J., Mao, R., Zhao, X., 2016. Possible influence of atmospheric circulations on winter haze pollution in the Beijing-Tianjin-Hebei region, northern China. *Atmos. Chem. Phys.* 16, 561–571.
- Zhong, J., Zhang, X., Wang, Y., Wang, Y.Q., Liu, C., Dong, Y.S., 2018. Heavy aerosol pollution episodes in winter Beijing enhanced by radiative cooling effects of aerosols. *Atmos. Res.* 209, 59–64.
- Zhou, M., Zhang, L., Chen, D., Gu, Y., Fu, T., Gao, M., et al., 2019. The impact of aerosol-radiation interactions on the effectiveness of emission control measures. *Environ. Res. Lett.* 14, 024002.